Journal of the Mechanical Behavior of Biomedical Materials 94 (2019) 10–18

Contents lists available at ScienceDirect

Journal of the Mechanical Behavior of Biomedical Materials

journal homepage: www.elsevier.com/locate/jmbbm

Light but tough bio-inherited materials: Luffa sponge based nickel-plated composites

Sha Yin[a,b,c], Huitian Wang[a,b], Jiani Li[a,b], Robert O. Ritchie[d,*], Jun Xu[a,b,**]

[a] Department of Automotive Engineering, School of Transportation Science and Engineering, Beihang University, Beijing 100191, China
[b] Advanced Vehicle Research Center (AVRC), Beihang University, Beijing 100191, China
[c] State Key Laboratory for Strength & Vibration of Mechanical Structures, School of Aerospace Engineering, Xi'an Jiaotong University, Xi'an 710049, China
[d] Materials Sciences Division, Lawrence Berkeley National Laboratory, & Department of Materials Science & Engineering, University of California, Berkeley, CA 94720, USA

ARTICLE INFO

Keywords:
Bio-inherited materials
Luffa sponge
Plating
Mechanical properties
Energy absorption

ABSTRACT

Natural structural materials featuring fine hierarchical architectures often display remarkable mechanical properties. To inherit the microstructures of biological materials, nickel-plated luffa sponges were fabricated through electrochemical deposition using natural luffa sponges as templates. Four groups of samples were processed based on nickel electroless and electroplating, and then characterized by X-ray diffraction and optical/scanning electron microscopy. Axial compression tests were performed to characterize the mechanical properties of the nickel-plated samples to compare with those of the original natural sponges. Results showed that a uniform layer of nickel was formed on the luffa fibers by electroless plating; conversely, by electroplating the nickel only minimal deposits were found on the inner luffa wall due to the uneven current distribution over the surface of sponge. Accordingly, electroless plating was deemed to be far more effective for metal deposition of materials with complex structures, such as luffa sponge. Alkali treatments prior to plating were found to be critical for subsequent mechanical performance and energy absorption capacity. The mechanical properties of nickel-plated samples surpass those of original luffa sponges, with the enhancement efficiency, *i.e.*, the ratio of specific stiffness and strength, being highest for electroless-plated samples with a prior alkali treatment. Specifically, their energy absorption capacity was far superior to that in other comparable materials. Using a power scaling law, an empirical relationship was derived which indicated that the bending-dominated behavior of the nickel-plated luffa sponges was similar to that of open-cell foams. We believe that other artificially "bio-inherited materials" could be successfully processed and developed in this manner. The superior properties of bio-inherited materials that we obtained in this work may provide inspiration for future research efforts on bio-inspired structural materials.

1. Introduction

Natural materials, featuring complex hierarchical, multiple length-scale, structures, often possess excellent combinations of mechanical properties surpassing those of their man-made counterparts (Gibson and Ashby, 1997; Gibson et al., 2010), despite the fact that they are processed at near-ambient temperatures from a limited palette of materials with relatively meager structural properties. Indeed, much research, especially over the past decade, has been focused on bioinspiration by exploring the natural design philosophies and delicate, often graded, structures in biological materials in order to mimic them to create new synthetic materials with unprecedented mechanical properties (Liu et al., 2018; Munch et al., 2008; Schaedler et al., 2011).

With respect to such mechanical properties, nacre from red Abalone shells has been one of the most studied natural materials, as it exhibits strong and flaw-tolerant characteristics resulting from its micro-scale brick-and-mortar structure (Bonderer et al., 2008). Analogously, the *Euplectella* glass sponge has a hierarchical construction achieved through a lengthy evolution process and guided by environmental constraints (Aizenberg et al., 2005; Meyers et al., 2011); as such, it represents another natural material that possesses exceptional mechanical stability and toughness. To mimic the microstructures of these natural materials, a wide variety of fabrication techniques, including mineralization (Ding et al., 2017), casting (Porter et al., 2013) and 3D

* Corresponding author.
** Corresponding author at: Department of Automotive Engineering, School of Transportation Science and Engineering, Beihang University, Beijing 100191, China.
E-mail addresses: roritchie@lbl.gov (R.O. Ritchie), junxu@buaa.edu.cn (J. Xu).

https://doi.org/10.1016/j.jmbbm.2019.02.029
Received 27 October 2018; Received in revised form 2 February 2019; Accepted 28 February 2019
Available online 01 March 2019
1751-6161/

printing (Studart, 2016; Velasco-Hogan et al., 2018), have been explored. However, few of these processing approaches have been able to closely mimic the natural structures with respect to their morphology, size-scales and the presence of gradients and graded interfaces. Indeed, it is difficult and costly to make engineering materials in the image of the fine and complex microstructures of biological materials, primarily because most synthetic processing techniques used to make bulk materials are "top-down", whereas natural processing is invariably "bottom-up" commencing with atomic and molecular manipulation. However, in this regard, synthetic architected materials have attracted some attention as they represent lightweight and multifunctional materials that can be constructed "bottom-up" from different constituents (Tancogne-Dejean et al., 2016; B. Xu et al., 2017; J. Xu et al., 2017) with different shapes (Schaedler et al., 2013; Xu et al., 2018a, 2018b; Yin et al., 2018, 2017). The mechanical properties of architected materials depend on their constituents, their architecture and/or combinations of the two, but there is no reason why their structures could not be further optimized and manipulated using bioinspired principles.

Luffa sponges, as a commercially viable natural-cellular materials, originate from *Luffa cylindrica*, a plant of cucurbitaceae family (Sinnott and Bloch, 1943). During their growth, the ovaries of luffa sponges differentiate into elongate cells and finally form a fibrous network. After the luffa fruit is fully mature, the pulp can be air dried naturally to leave a scaffold of fibers consisting of cellulose, hemicellulose and lignin (Chen et al., 2018; Tanobe et al., 2005). To examine the mechanical properties of such luffa sponges, Shen et al. (2012, 2013, 2014) considered both quasi-static and dynamic loading conditions, and found that the compressed sponges were recoverable after immersing in water and sensitive to loading rate, yet had excellent energy absorption potential. In particular, Chen et al. (2014) found that during compression the inner surfaces of sponge play a prime role in supporting the axial loads. However, natural luffa sponges have been utilized as templates to develop functional as well as structural materials. For example, Alshaaer et al. (2017) used luffa fibers as a template to fabricate porous bioceramics for the application of bone tissue, whereas Zampieri et al. (2006) similarly fabricated hierarchical zeolite for use as catalytic reactors.

The objective of this work is to develop, what we term, "bio-inherited" materials using luffa sponges as template with simple metallic electrochemical deposition, and to examine their corresponding mechanical performance. We create a series of novel composite materials consisting of nickel-plated luffa sponges, using both electroless and electroplating, characterize their multi length-scale structures, using optical and scanning electron microscopy (SEM) and X-ray diffraction (XRD), and determine their mechanical properties with uniaxial compression tests, to provide a comparison with the structure and properties of natural luffa sponges and other comparable materials.

2. Experimental

2.1. Samples

2.1.1. Raw materials

All the luffa sponges in this work were obtained from luffa fruits that were grown in the Zhejiang Province of China (Fig. 1a,b); they were procured by removing the skin and seeds after natural drying, before being cut into segments, as shown in Fig. 1c. The sponges were cut into ~40 mm long column samples, which were then milled with angle grinder to ensure that the two end surfaces were parallel. The column samples were water rinsed and then soaked in deionized water to remove dust and seeds. Fig. 1d shows a luffa sponge after preprocessing. The structure of the sponge mainly comprises a luffa wall, voids and an inner core portion. From the cross-sections, typically two to four voids can be found in the luffa sponges; accordingly, to exclude the influence of void number, sponges with only three voids were used in this research. By ignoring the voids and taking the end faces as perfect circles, the luffa columns could be approximated as truncated cones, with measured diameters ranging from 53.3 to 69.8 mm and a height ranging from 35.0 to 41.4 mm (the average height was 38.5 mm). The densities were then defined as the measured weights over the volumes of the sponges as truncated cones.

2.1.2. Electrochemical deposition

Electroless plating and electroplating of nickel were employed using the luffa sponges as templates. The luffa sponges consist of cellulose wrapped by lignin and hemicellulose (Chen et al., 2018; Tanobe et al., 2005). Only the cellulose molecular chains rich of hydroxyl groups can facilitate the formation of hydrogen bonds between the cellulose and aqueous solution (Song et al., 2018). To improve the hydrophilic nature of the luffa fibers, 8% (w/w) NaOH solution was used to eliminate the lignin and hemicellulose (Chen et al., 2018; Ghali et al., 2009; Tanobe et al., 2005). The alkali treatment was performed for 1 h under water bath at 90 °C, whereupon the samples were rinsed in water for 10 mins to remove the remaining NaOH. Meanwhile, luffa sponges with purer ingredient were obtained.

The luffa sponges were sensitized and successively activated by respectively soaking in stannous chloride solution (10 g/L) and palladium chloride solution (0.5 g/L), both for 5 mins (Fan et al., 2018; Schlesinger and Paunovic, 2010). Then, the activated luffa sponges were dried in air at room temperature for 24 h to ensure the stability of plating solution during electroless plating, prior to being moved into the plating solution for the actual electroless plating. By controlling the plating time from 10 mins to 2 h, nickel-plated samples were obtained with varying densities, as shown in Fig. 1e. Electroplating was subsequently performed, continuously for 90 mins at a current of 1.5 A, on electroless plated samples. A luffa sponge after such electroplating is shown in Fig. 1f.

All the samples were separated into six groups based on their fabrication, as indicated in Table 1; this involved group O (original luffa sponges), group AO (luffa sponges with alkali treatment), group C (electroless plated luffa sponges), group AC (electroless plated luffa sponges with alkali treatment), group E (electroplated luffa sponges), and group AE (electroplated luffa sponges with alkali treatment).

2.2. Characterization

Optical microscopy and scanning electron microscopy (SEM, HITACHI S-4800) were used to characterize the morphology of the luffa fibers before and after electrochemical plating. X-ray diffraction (XRD) was performed on all groups to characterize the chemical component of all samples with different fabrication processes.

2.3. Compression tests

Uniaxial compression tests of all the samples were conducted on an Instron 2345 electromechanical universal testing machine (Instron Corp., Norwood, MA) at a strain rate of 10^{-3} s^{-1}. The displacement rate varied marginally at ~2.4 mm/min because the heights of luffa columns were not rigidly 40 mm after mill and alkali treatment.

3. Results and discussion

3.1. Morphology

As mentioned before, luffa sponges have several voids among fibrous network. The voids can reduce material weight, and the core parts separating the voids can improve the stability of the fibrous cylinder. Observations shown in Fig. 2 revealed that the morphology of core consists of fiber networks with many pores for growth of the seeds (Fig. 2a). Whereas the luffa wall displays different morphologies at the outside and inside of the wall (Fig. 2b); images of these inner and outer wall surfaces are given in Fig. 2c,d, respectively, with blue markers

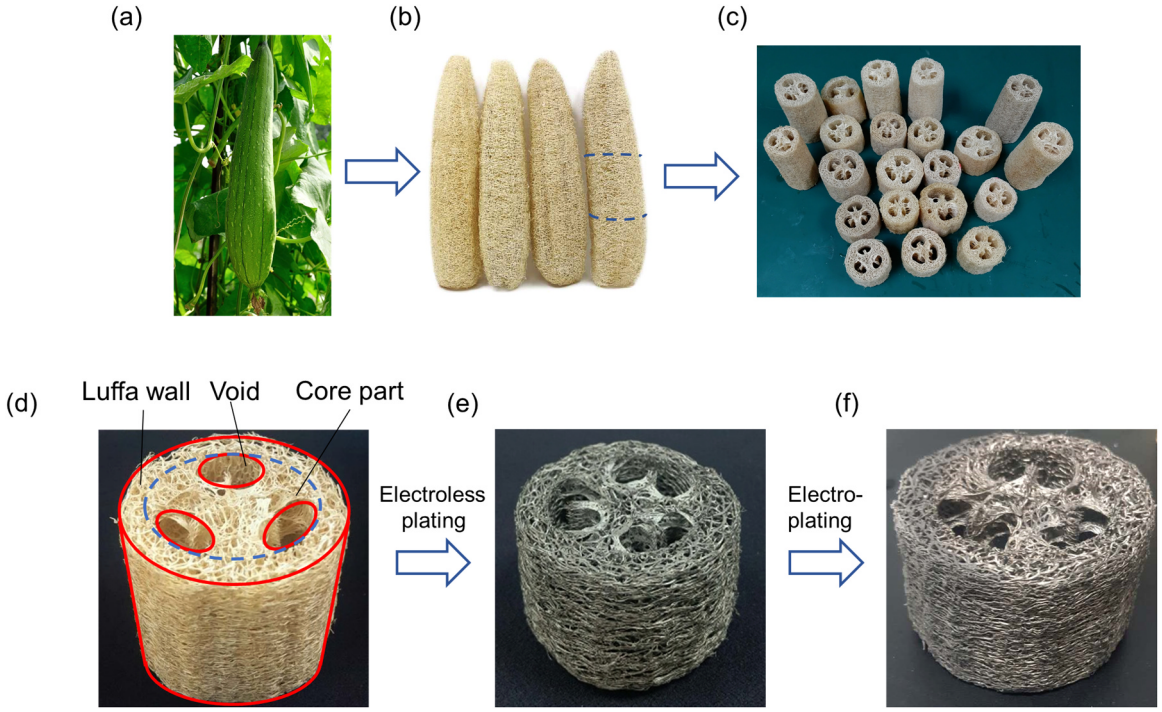

Fig. 1. (**a**) Immature luffa fruits; (**b**) mature luffa fruits (luffa sponges); (**c**) luffa columns processed from raw luffa sponges; (**d**) original luffa sponge sample used in this work; (**e**) electroless plated luffa sponge and (**f**) electroplated luffa sponge.

Table 1
Fabrication details of the six groups of luffa sponges in this study.

Group name	Alkali treatment	Sensitization + Activation	Electroless plating	Electroplating
O	–	–	–	–
C	–	✓	✓	–
E	–	✓	✓	✓
AO	✓	–	–	–
AC	✓	✓	✓	–
AE	✓	✓	✓	✓

indicating the fiber orientations. The inner surface consists of axial fibers with aligned interconnecting fibers to form a fiber network; the outer surface consists of circumferential fibers that are mainly loosely organized together. Note that the fibers on the inner surface are much stouter than those on the outer one, which makes the inner surface stiffer. The surface of the inner wall displayed little difference in morphology before and after alkali treatment (Fig. 2e-h); both had an intact net-like structure with no obvious damage on the fiber surface. However, the luffa fibers became ~30% finer and ~14% lighter after the alkali treatment.

For the nickel-plated luffa sponges, the luffa wall was cut to examine its morphology (Fig. 3). A uniform layer of nickel with a silver color can be seen on the fibers along the inner and outer surfaces of the electroless plated luffa sponges, as shown in Fig. 3a–c. For the corresponding electroplated sponges, most of the inner surface of the wall also exhibited a silver color (Fig. 3f,h), although the marginal part (Fig. 3i) and outer surface (Fig. 3g,j) displayed a color of matte gray, which is the characteristic of electroplated nickel. This indicates that nickel was not adequately deposited on the inner wall surface.

The deposited layer thickness at any point on the surface of an article being electroplated is dependent on the current density at that point; in turn, the current density is determined by the distribution of the current over the surface of the article, which is largely influenced by geometric factors (Schlesinger and Paunovic, 2010). The inner surfaces of the luffa wall are surrounded by the whole luffa sponge, which thus makes deposition difficult. During the electroplating process, mechanical stirring was employed to assist the uniformity of the nickel layer; nevertheless, most of the inner surfaces of the walls remained unplated.[1]

Comparing the state of the nickel deposition of the luffa fibers on the outer surface of the electroless-plated and electroplated sponges (Fig. 3), it was apparent that the surfaces of nickel-plated fibers in the electroless-plated samples were smoother and more even (Fig. 3d), whereas they were quite rough for electroplated samples with evidence of aggregates of nickel particles (Fig. 3k). Additionally, the micron-scale nickel particles produced by electroplating were much sharper than those produced by electroless plating, as shown in Fig. 3e,l.

XRD intensity distribution patterns for the samples from the six groups are presented in Fig. 4. By comparing the XRD results for natural sponges in groups O and AO, nickel-plated sponges by electroless plating in groups C and AC, and those by electroplating in groups E and AE (see Table 1), no obvious influence was found of the alkali treatment on the crystal structure and chemical composition of the samples. For groups O and AO, the two diffraction peaks can be identified at ~16° and 20° which can be ascribed to the cellulose (Tong et al., 2014). For groups C and AC, additionally three diffraction peaks were observed at ~44.5°, 51.8° and 76.4° corresponding to the characteristic peaks of nickel. For groups E and AE, all these five peaks were observed but the

[1] The problem can probably be alleviated with methods used in industrial production such as shells cathode movement which act to improve the current distribution (Schlesinger and Paunovic, 2010).

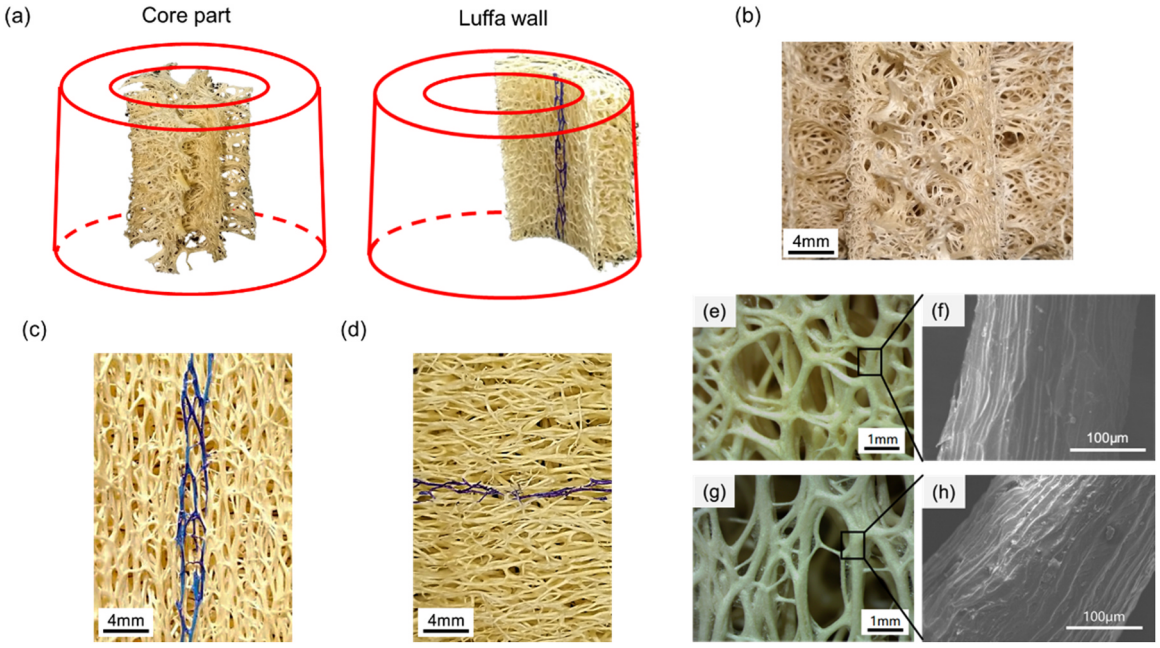

Fig. 2. (**a**) Illustration of the core part and luffa wall of the luffa sponge. Morphology of the (**b**) core part (**c**) inner surface and (**d**) outer surface of luffa wall. Optical and SEM micrographs for inner surface morphology of (**e-f**) luffa sponge and (**g-h**) alkali-treated luffa sponge.

intensity of nickel peaks was reduced, indicative of the disorder and smaller grain size of nickel crystals produced by electroplating.

3.2. Mechanical properties: compression tests

Representative compressive stress-strain curves for each group of samples are compared in Fig. 5a. For the natural sponges in group O, a three-stage curve, typical of cellular materials, was observed, with a rapid initial linear elastic stage leading to a constant plateau followed by a densification stage. Similar stress-strain curves were measured for the other groups, and they share the same deformation mode corresponding to the deformation history shown in Fig. 5b. In the elastic stage, all samples deformed uniformly up to an initial stress peak, before undergoing a small load drop which could be attributed to buckling of the inner wall surface. Localized densification originated randomly from where the fibrous network was sparse. Fig. 5c shows sample cross-section after compression. Folding of the inner surface with no fractured fibers was observed; the fibrous network in this region exhibited integrated deformation during the compression.

During the stress-strain curves for a small portion of samples without alkali treatment (curve E' in Fig. 5a), the stress can be seen to drop sharply after an initial peak followed by numerous fluctuations throughout the plateau stage. Localized shear bands were observed after the stress drop, and then the fibers fractured with further compression, accompanying by numerous fragments falling from the samples (Fig. 5d). Fig. 5e shows the fractured fibers in the inner surface, indicative of the brittleness induced by inappropriate processing (*e.g.* over-drying). It is this fracture of the fibrous network that causes the severe drop in stress after the initial stress peak. This deformation mode naturally is inconsistent for use in energy absorption applications.

3.3. Compressive stiffness and strength

The compressive strength values of all samples were equated to the initial peak stress or the stress at the intersection of slopes of the linear and plateau stages. The slope between 25% and 75% of the compressive strength was taken to represent the compressive stiffness (Shen et al., 2012). The calculated stiffness and strength of all the six groups were plotted against their densities in Fig. 6a,b. The samples with and without alkali treatment after electroless plating (group C and AC) performed rather similarly. However, the alkali-treated luffa sponges had a 14% decrease in mass, and the extent of their elevation in mechanical properties after electrodeposition was clearly different to that of the untreated sponges. The complex ingredients of natural materials (including cellulose, lignin and hemicellulose) have made the fabrication process different from that of man-made materials which usually have single raw materials, and thus the mechanical properties attained with large variation and sometimes do not even outperform the original materials. However, in order to further examine the feasibility by creating novel materials by electrodeposition, and explore the deformation mechanism and structure-mechanical property relationships of the bio-inherited materials, we subsequently focus on the treated luffa sponges with purer ingredient in this study.

To quantify the enhancement effect, the average stiffness or strength values in each group were used to make the comparison. For each plated group, these two values were compared with those from the corresponding original groups, *i.e.* those without alkali treatment (groups C and E) are compared with group O, while for those with alkali treatment (groups AC and AE) are compared with group AO. The ratios of the average stiffness E and strength σ in each group and their corresponding original groups, are denoted as ξ_E and ξ_σ. Meanwhile, the ratios of the average specific stiffness E/ρ and strength σ/ρ are also introduced, denoted as $\eta_{\bar{E}}$ and $\eta_{\bar{\sigma}}$ to depict the enhancement efficiency considering the mass increment after nickel deposition.

All these representative parameters are summarized and compared in Fig. 6c,d. The results indicate that the stiffness and strength values of nickel-plated luffa sponges surpass those of their original ones, and increase with nickel film thickness. In terms of their stiffness and strength, the alkali-treated, nickel-electroless and electro-plated sponges from group AE displayed the best properties while the non-alkali-treated, electroless-plated (only) sponges from group C were the worst. However, the alkali-treated and electroless-plated (only) luffa sponges from group AC exhibited the maximum increase of specific stiffness and strength, as compared to those from the corresponding natural samples in group AO. In general, the stiffness and strength of the electroplated sponges were quite varied; indeed, most of the

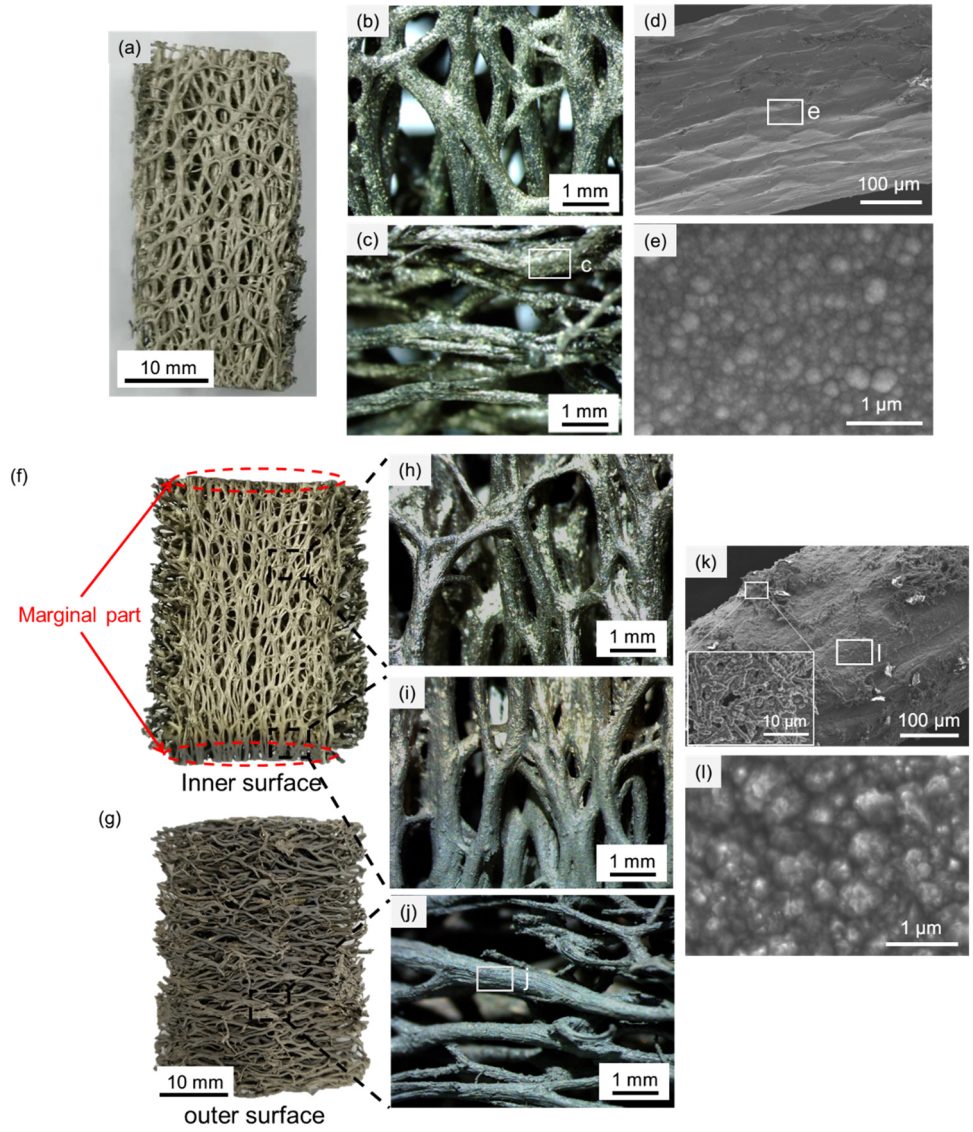

Fig. 3. Morphology of the electroless-plated luffa sponges: optical images for (**a**-**b**) inner and (**c**) outer surface; (**d**-**e**) SEM images for fiber surface morphology. Morphology of the electroplated luffa sponges: optical images for (**f**) inner and (**g**) outer surfaces; the nickel-plated fibers from the (**h**) middle part and (**i**) marginal part of the inner surface and those from the (**j**) outer surface; (**k**-**l**) SEM images of the fiber surface morphology (inset: aggregation of nickel particles), respectively.

samples did not exhibit any real enhancement in mechanical properties. We attribute this to the uneven layer of nickel deposited on luffa sponges, especially that not much nickel was deposited on the inner surface of the walls which is in general the stiffest part of the sponge. However, the comparisons between the various groups with respect to their strength and stiffness did indicate that the alkali treatments were critically important for achieving the best mechanical properties of the nickel-deposited natural fibers, which should be attributed to the better interfacial adhesion after treatment between natural fiber (cellulose) and nickel.

In general, the compressive stiffness and strength of cellular materials follow a power scaling law with the relative density, which can be expressed as:

$$E = A_1 \rho^{B_1}, \tag{1}$$

$$\sigma = A_2 \rho^{B_2}, \tag{2}$$

where E and σ are the compressive stiffness and strength of nickel-plated luffa sponges, ρ is the density, and A and B are material parameters. For group AC which exhibits the best enhancement efficiency, the fitting curves of compressive strength and stiffness as a function of density are shown in Fig. 6c,d. For cellular materials with different deformation modes, parameters B_1 and B_2 are different, and can be generally classified into two types, *i.e.* stretching-dominated and bending-dominated. From existing literature, the exponents B_1 and B_2 are equal to 1 for stretching-dominated materials, and the truss materials will fail in the form of plastic yielding. Specifically, if the relative density of cellular material is low enough, the truss will fail by elastic buckling and B_2 will change into 2 (Elsayed and Pasini, 2010). While for bending-dominated materials, B_1 and B_2 are given by 2 and 1.5 respectively; here the structure will fail in the form of plastic collapse (Deshpande et al., 2001). We analyze the mechanism both through the value of the exponents and by deformation mode. As shown in Fig. 6e,f, by fitting the experimental data of group AC, empirical formulas in the form of Eqs. (1 and 2) can be obtained, and B_1 and B_2 are 1.89 and 1.56, respectively, which are closer to the exponents for bending-dominated materials. Additionally, as shown in Fig. 5c, the fiber network of nickel-plated luffa sponges bent and folded after compression, which is similar to open-cell foams that are governed by cell wall bending at all loading conditions. Therefore, we came to the conclusion that the nickel-plated luffa sponges in this study can be termed as bending-dominated materials like open-cell foams.

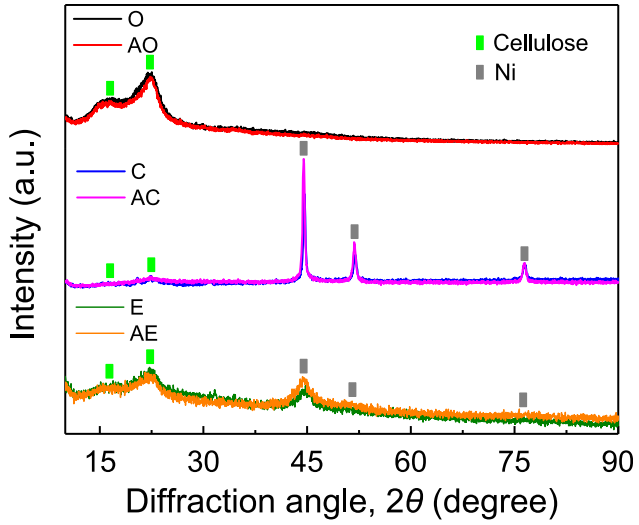

Fig. 4. X-ray diffraction patterns for the original, electroless plated and electroplated luffa sponges, before and after alkali treatment.

Comparing with those from group AC, the ingredients of samples from group C without alkali treatment are complex including cellulose, lignin, hemicellulose and nickel. The corresponding stiffness and strength values of group C are also plotted in Fig. 6g,h, which are hardly to fit into a straight line, indicating the dispersion and irregularity of mechanical properties. Thus, alkali treatment is essential for excluding the constituent complexity and for exploring mechanical property-structure relationships.

3.4. Energy absorption

One measure of the energy absorption capacity can be characterized by the energy dissipated during the compression test. Energy absorption (EA) capacity per unit volume is defined from the area under the stress-strain curve as:

$$W_v = \int_0^{\varepsilon_D} \sigma \mathrm{d}\varepsilon, \tag{3}$$

where ε_D is the densification strain, and the corresponding energy absorption per unit mass is given by $W_m = W_v/\rho$. Effectively this is a measure of the toughness of the material. An energy absorption efficiency method (Avalle et al., 2001) is used to calculate the densification strain. Specifically, the energy absorption efficiency, $\Psi(\varepsilon)$, is defined as:

$$\Psi(\varepsilon) = \frac{\int_0^{\varepsilon} \sigma(\varepsilon)\mathrm{d}\varepsilon}{\sigma(\varepsilon)}, \tag{4}$$

with the densification strain taken as the strain where $\Psi(\varepsilon)$ reaches a maximum value, satisfying:

$$\left.\frac{d\Psi(\varepsilon)}{\mathrm{d}\varepsilon}\right|_{\varepsilon=\varepsilon_D} = 0. \tag{5}$$

The plateau stress can then be calculated as $\sigma_p = W/\varepsilon_D$. Fig. 7a illustrates how the calculation of the densification strain and plateau stress is performed from the compressive stress-strain curve.

The calculated specific energy absorption and plateau stress values of all the samples are plotted against their densities in Fig. 7b,c. For those sponges with prior alkali treatment, as expected the EA capacity was found to increase significantly after deposition, as compared to that of the original natural sponges; without the alkali treatment, the EA was essentially unchanged. Again, group AC sponges displayed the best mechanical properties, with the highest enhancement efficiency of the EA capacity of all the sponges. The plateau stress of certain samples, particularly those in group E which failed by localized shear band formation, decreased markedly with strength, which naturally resulted in poor EA values. Indeed, the trends in the EA and plateau stress with density (Fig. 7b,c) were quite similar to those observed above for the strength and stiffness (Fig. 6).

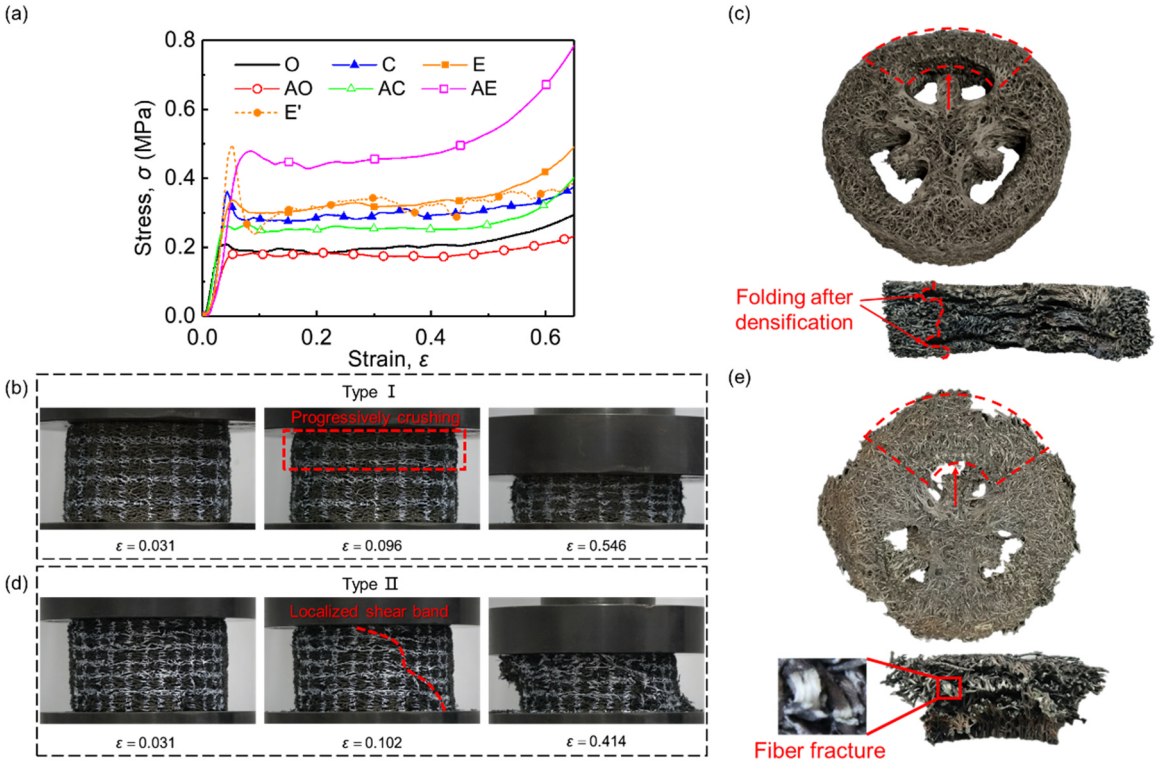

Fig. 5. (**a**) Typical compressive stress-strain curves of the nickel-plated luffa sponges, as compared to those for natural sponges. Deformation histories and the corresponding failure modes of two types of samples: (**b–c**) type I (**d–e**) type II.

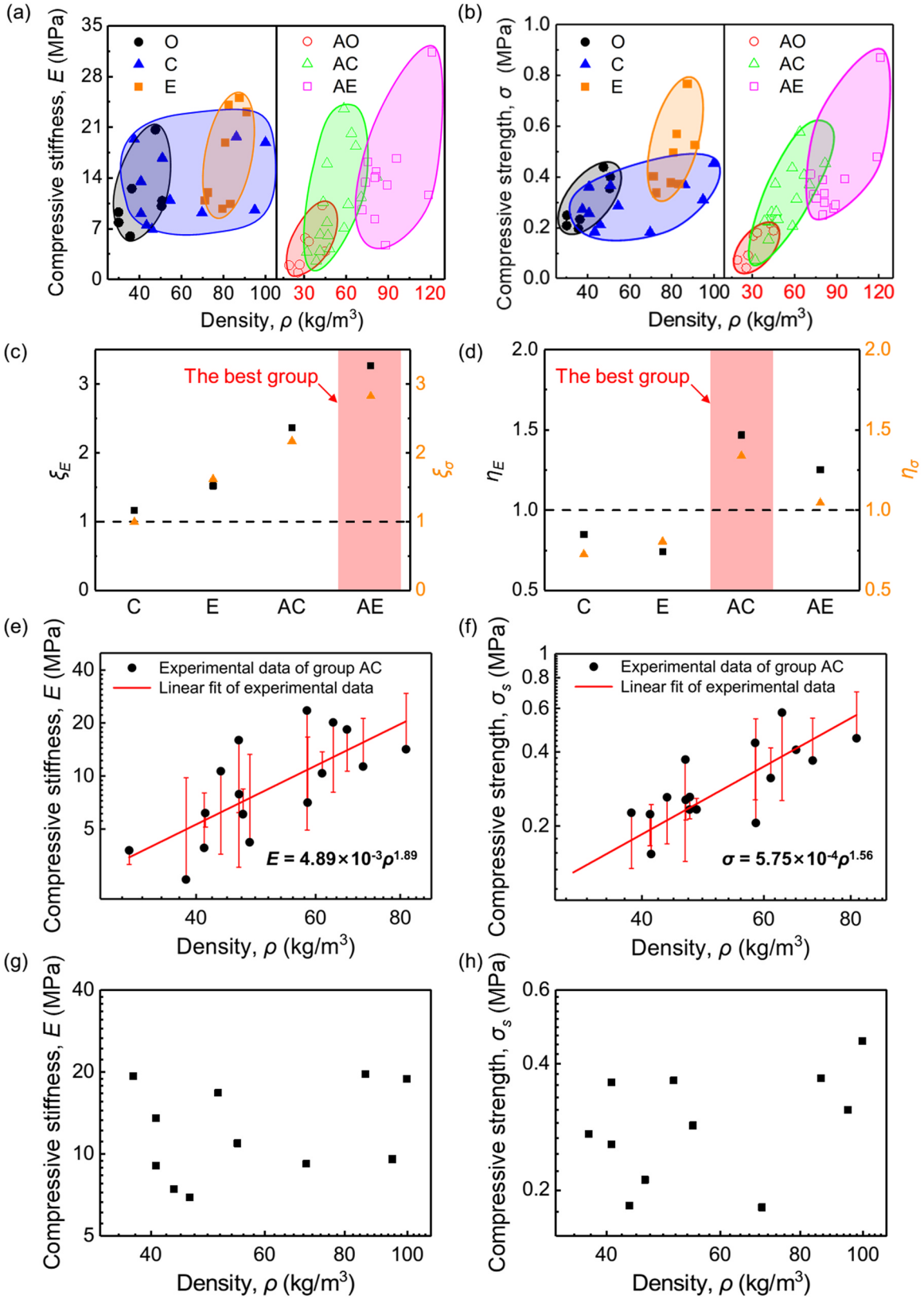

Fig. 6. (**a**) Compressive stiffness and (**b**) strength of nickel-plated luffa sponges as compared with the natural ones. The ratios of (**c**) the average stiffness and strength, (**d**) the average specific stiffness and strength of nickel-plated luffa sponges in each group comparing with the corresponding original ones. Fitting of (**e**) stiffness and (**f**) strength for samples of group AC, and the scatter plot of (**g**) stiffness and (**h**) strength for samples of group C.

The energy absorption of these nickel-plated luffa sponges is plotted in an Ashby chart, and compared with other lightweight cellular materials in Fig. 8. The bio-inherited materials are superior to aluminum foam (Ashby et al., 2000), and meanwhile can be comparable with CFRP honeycombs (George et al., 2014) and stainless-steel lattice (Ullah et al., 2016). Specifically, compared with these the comparable

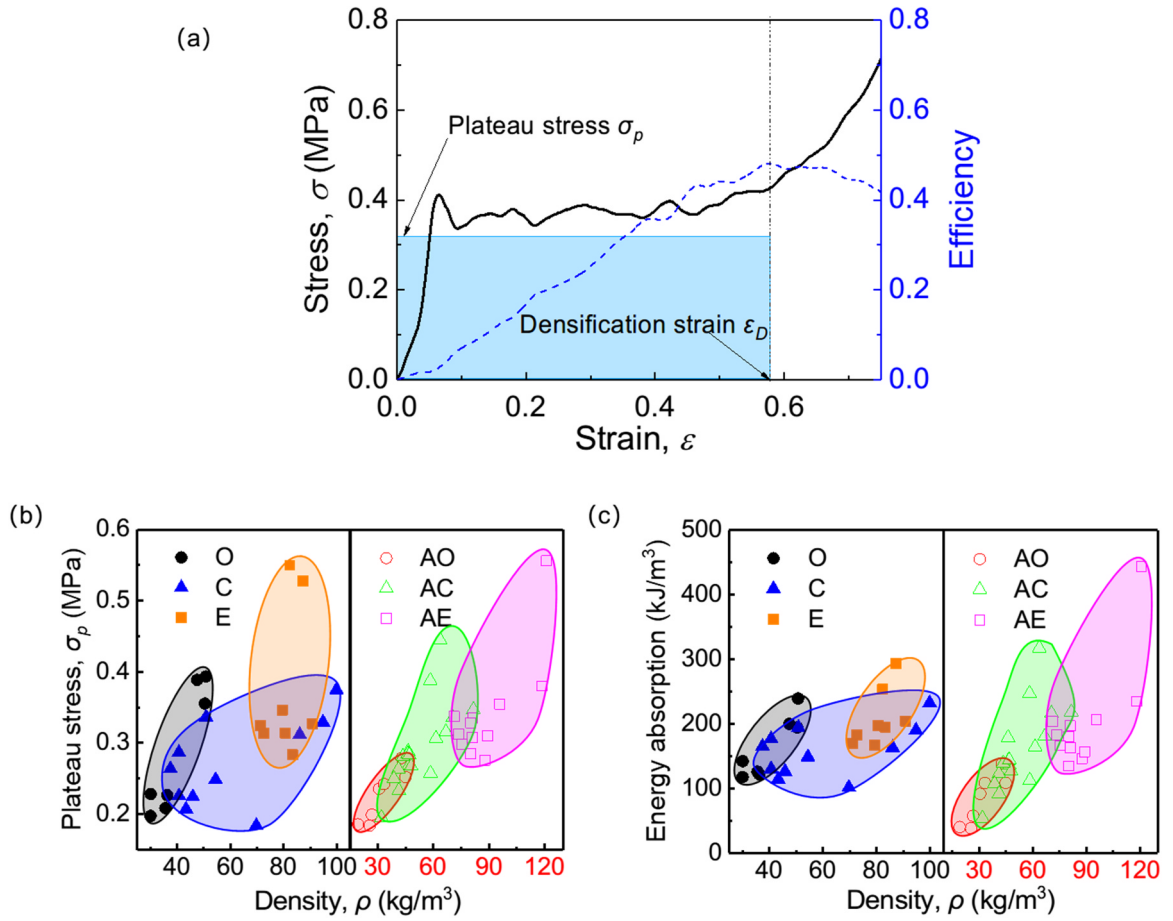

Fig. 7. (**a**) Illustration of the energy absorption (EA) efficiency method; (**b**) plateau stress and (**c**) EA of the nickel-plated and original luffa sponges as a function of their density.

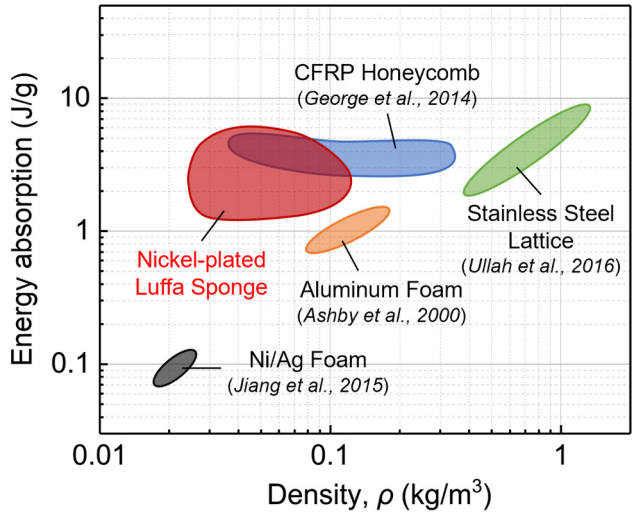

Fig. 8. Ashby chart about the energy absorption of nickel-plated luffa sponges compared with other cellular materials.

materials, Ni/Ag foams are fabricated in the same way by electrochemical deposition on polymer foams. However, the energy absorption is far less than that of nickel-plated luffa sponges (Jiang et al., 2015). The density contrast in the Ashby chart can aid the selection of appropriate materials in a specific density range. The steady deformation and good energy absorption capacity of luffa sponges can be attributed to their structural characteristics and material gradients that are established in their architecture.

4. Conclusions

Nickel-plated luffa sponges, that inherit the fiber-network microstructures of natural luffa sponges, have been successfully fabricated by electroless plating and electroplating. The morphology and mechanical properties were characterized by SEM, XRD and uniaxial compression tests. Compressive stiffness, strength, plateau stress and energy absorption capacity have been investigated and compared with other competing materials. Based on this work, the following conclusions can be made:

1. Due to the complex geometry of luffa sponges, electroless plating provided a more reliable method for depositing nickel on the sponges than electroplating; the latter process depended on the distribution of the current which tended to be uneven over the luffa walls leading to areas that were only marginally plated. By controlling the deposition time, those with variable nickel film thickness could be obtained. Moreover, prior alkali treatment was vital in improving the nickel coating on the natural fibers and to guarantee the excellent mechanical properties of the nickel-plated luffa sponges.
2. Reliable nickel deposition could definitively enhance the compressive stiffness and strength of the luffa sponges, with prior alkali-treated sponges having superior properties to those that were not alkali-treated. Those with a thicker nickel film performed better; however, in terms of the enhancement efficiency (the property

increment over the mass increment), electroless-plated luffa sponges with prior alkali treatment performed the best among four groups.
3. By fitting an empirical power law of stiffness and strength to the experimental data, nickel-plated luffa sponges behave more like bending-dominated materials. In terms of the toughness properties, the energy absorption capacity of these bio-inherited materials can be superior to many man-made engineering materials, such as aluminum foam and metallic lattice materials.

The superior properties of bio-inherited materials attained, should be mainly attributed to the specific microstructure of luffa sponges, which will lead us more future research efforts on bio-inspired works.

Acknowledgments

J.X. and S.Y. were financially supported by the National Key Research and Development Program of China (2017YFB0103703), Chinese Academy of Space Technology (CAST-BISEE2017-021), Young Elite Scientist Sponsorship Program by CAST, and Opening fund of State Key Laboratory for Strength and Vibration of Mechanical Structures, Xi'an Jiaotong University (SV2016-KF-20). R.O.R. was funded by the Mechanical Behavior of Materials Program (KC13) at the Lawrence Berkeley National Laboratory, supported by the U.S. Department of Energy, Office of Science, Office of Basic Energy Sciences, Materials Sciences and Engineering Division, under contract No. DE-AC02–05CH11231.

References

Aizenberg, J., Weaver, J.C., Thanawala, M.S., Sundar, V.C., Morse, D.E., Fratzl, P., 2005. Skeleton of Euplectella sp.: structural hierarchy from the nanoscale to the macroscale. Science 309, 275–278.
Alshaaer, M., Kailani, M.H., Ababneh, N., Abu Mallouh, S.A., Sweileh, B., Awidi, A., 2017. Fabrication of porous bioceramics for bone tissue applications using luffa cylindrical fibres (LCF) as template. Process. Appl. Ceram. 11, 13–20.
Ashby, M.F., Evans, A.G., Fleck, N.A., Gibson, L.J., Hutchinson, J.W., Wadley, H.N.G., 2000. Metal Foams: a Design Guide. Butterworth-Heinemann, Warrendale.
Avalle, M., Belingardi, G., Montanini, R., 2001. Characterization of polymeric structural foams under compressive impact loading by means of energy-absorption diagram. Int. J. Impact Eng. 25, 455–472.
Bonderer, L.J., Studart, A.R., Gauckler, L.J., 2008. Bioinspired design and assembly of platelet reinforced polymer films. Science 319, 1069–1073.
Chen, Q., Shi, Q., Gorb, S.N., Li, Z., 2014. A multiscale study on the structural and mechanical properties of the luffa sponge from Luffa cylindrica plant. J. Biomech. 47, 1332–1339.
Chen, Y., Su, N., Zhang, K., Zhu, S., Zhu, Z., Qin, W., Yang, Y., Shi, Y., Fan, S., Wang, Z., Guo, Y., 2018. Effect of fiber surface treatment on structure, moisture absorption and mechanical properties of luffa sponge fiber bundles. Ind. Crop. Prod. 123, 341–352.
Deshpande, V.S., Ashby, M.F., Fleck, N.A., 2001. Foam topology bending versus stretching dominated architectures. Acta Mater. 49, 1035–1040.
Ding, C., Chen, Z., Li, J., 2017. From molecules to macrostructures: recent development of bioinspired hard tissue repair. Biomater. Sci. 5, 1435–1449.
Elsayed, M.S.A., Pasini, D., 2010. Multiscale structural design of columns made of regular octet-truss lattice material. Int. J. Solids Struct. 47, 1764–1774.
Fan, Q., Gao, Y., Zhao, Y., Yang, Q., Guo, L., Jiang, L., 2018. Fabrication of diamond-structured composite materials with Ni-P-diamond particles by electroless plating. Mater. Lett. 215, 242–245.
George, T., Deshpande, V.S., Sharp, K., Wadley, H.N.G., 2014. Hybrid core carbon fiber composite sandwich panels: fabrication and mechanical response. Compos. Struct. 108, 696–710.
Ghali, L., Msahli, S., Zidi, M., Sakli, F., 2009. Effect of pre-treatment of Luffa fibres on the structural properties. Mater. Lett. 63, 61–63.
Gibson, L.J., Ashby, M.F., 1997. Cellular Solids Structure and Properties, first ed. Cambridge University Press, Cambridge.
Gibson, L.J., Ashby, M.F., Harley, B.A., 2010. Cellular materials in nature and medicine, first ed. Cambridge University Press, Cambridge.
Jiang, B., He, C., Zhao, N., Nash, P., Shi, C., Wang, Z., 2015. Ultralight metal foams. Sci. Rep. 5, 13825.
Liu, J., Li, H., Zhang, H., Liu, Q., Li, R., Li, B., Wang, J., 2018. Three-dimensional hierarchical and interconnected honeycomb-like porous carbon derived from pomelo peel for high performance supercapacitors. J. Solid. State Chem. 257, 64–71.
Meyers, M.A., Chen, P.Y., Lopez, M.I., Seki, Y., Lin, A.Y., 2011. Biological materials: a materials science approach. J. Mech. Behav. Biomed. Mater. 4, 626–657.
Munch, E., Launey, M.E., Alsem, D.H., Saiz, E., Tomsia, A.P., Ritchie, R.O., 2008. Tough, bio-inspired hybrid materials. Science 322, 1516–1520.
Porter, M.M., McKittrick, J., Meyers, M.A., 2013. Biomimetic materials by freeze casting. JOM 65, 720–727.
Schaedler, T.A., Jacobsen, A.J., Carter, W.B., 2013. Toward lighter, Stiffer materials. Science 341, 1181–1182.
Schaedler, T.A., Jacobsen, A.J., Torrents, A., Sorensen, A.E., Lian, J., Greer, J.R., Valdevit, L., Carter, W.B., 2011. Ultralight metallic microlattices. Science 334, 962–965.
Schlesinger, M., Paunovic, M., 2010. Modern Electroplating, fifth ed. John Wiley & Sons, Inc, New Jersey.
Shen, J., Xie, Y.M., Huang, X., Zhou, S., Ruan, D., 2012. Mechanical properties of luffa sponge. J. Mech. Behav. Biomed. Mater. 15, 141–152.
Shen, J., Xie, Y.M., Huang, X., Zhou, S., Ruan, D., 2013. Behaviour of luffa sponge material under dynamic loading. Int. J. Impact Eng. 57, 17–26.
Shen, J.H., Xie, Y.M., Zhou, S.W., Huang, X.D., Ruan, D., 2014. Water-responsive rapid recovery of natural cellular material. J. Mech. Behav. Biomed. Mater. 34, 283–293.
Sinnott, E.W., Bloch, R., 1943. Development of the fibrous net in the fruit of various races of luffa cylindric. Bot. Gaz. 105, 90–100.
Song, J., Chen, C., Zhu, S., Zhu, M., Dai, J., Ray, U., Li, Y., Kuang, Y., Li, Y., Quispe, N., Yao, Y., Gong, A., Leiste, U.H., Bruck, H.A., Zhu, J.Y., Vellore, A., Li, H., Minus, M.L., Jia, Z., Martini, A., Li, T., Hu, L., 2018. Processing bulk natural wood into a high-performance structural material. Nature 554, 224–228.
Studart, A.R., 2016. Additive manufacturing of biologically-inspired materials. Chem. Soc. Rev. 45, 359–376.
Tancogne-Dejean, T., Spierings, A.B., Mohr, D., 2016. Additively-manufactured metallic micro-lattice materials for high specific energy absorption under static and dynamic loading. Acta Mater. 116, 14–28.
Tanobe, V.O.A., Sydenstricker, T.H.D., Munaro, M., Amico, S.C., 2005. A comprehensive characterization of chemically treated Brazilian sponge-gourds (Luffa cylindrica). Polym. Test. 24, 474–482.
Tong, Y., Zhao, S., Ma, J., Wang, L., Zhang, Y., Gao, Y., Xie, Y.M., 2014. Improving cracking and drying shrinkage properties of cement mortar by adding chemically treated luffa fibres. Constr. Build. Mater. 71, 327–333.
Ullah, I., Brandt, M., Feih, S., 2016. Failure and energy absorption characteristics of advanced 3D truss core structures. Mater. Des. 92, 937–948.
Velasco-Hogan, A., Xu, J., Meyers, M.A., 2018. Additive manufacturing as a method to design and optimize bioinspired structures. Adv. Mater. e1800940.
Xu, B., Yin, S., Wang, Y., Li, H., Zhang, B., Ritchie, R.O., 2017a. Long-fiber reinforced thermoplastic composite lattice structures: fabrication and compressive properties. Compos. Part a-Appl. 97, 41–50.
Xu, J., Gao, X., Zhang, C., Yin, S., 2017b. Flax fiber-reinforced composite lattice cores: a low-cost and recyclable approach. Mater. Des. 133, 444–454.
Xu, J., Wu, Y., Gao, X., Wu, H., Nutt, S., Yin, S., 2018a. Design of composite lattice materials combined with fabrication approaches. J. Compos. Mater. 0 (0021998318785710).
Xu, J., Wu, Y., Wang, L., Li, J., Yang, Y., Tian, Y., Gong, Z., Zhang, P., Nutt, S., Yin, S., 2018b. Compressive properties of hollow lattice truss reinforced honeycombs (Honeytubes) by additive manufacturing: patterning and tube alignment effects. Mater. Des. 156, 446–457.
Yin, S., Chen, H., Wu, Y., Li, Y., Xu, J., 2018. Introducing composite lattice core sandwich structure as an alternative proposal for engine hood. Compos. Struct. 201, 131–140.
Yin, S., Li, J., Liu, B., Meng, K., Huan, Y., Nutt, S.R., Xu, J., 2017. Honeytubes: hollow lattice truss reinforced honeycombs for crushing protection. Compos. Struct. 160, 1147–1154.
Zampieri, A., Mabande, G.T.P., Selvam, T., Schwieger, W., Rudolph, A., Hermann, R., Sieber, H., Greil, P., 2006. Biotemplating of Luffa cylindrica sponges to self-supporting hierarchical zeolite macrostructures for bio-inspired structured catalytic reactors. Mater. Sci. Eng.-C 26, 130–135.